



OPEN

Liquid crystal-based reconfigurable antenna for 5G millimeter-wave

Peng Chen¹, Dan Wang¹, Lihua Wang^{2✉}, Lu Liu¹ & Zongsheng Gan¹

This paper proposed a frequency reconfigurable antenna that utilizes a multilayer structure of liquid crystal (LC) material. This antenna design incorporates a three-layer stacked structure to create an LC-injected cavity. The inverted microstrip line structure is designed to be in contact with the LC, serving as both a radiating element and a bias electrode. A parasitic patch is placed at the top of the antenna to enhance bandwidth. To prevent interference with DC and RF sources, a bias tee is integrated into the microstrip line input. Experimental results demonstrate that the proposed antenna exhibits excellent impedance matching and stable radiation patterns within the operational frequency range. By comparing the simulated performance of the existing LC antenna with our proposed design, the bandwidth is tripled at a center frequency of 30.3 GHz. In addition, the effective area of the proposed reconfigurable antenna (154 mm²) is 24.6% of the area of the previous reconfigurable antenna (625 mm²).

Frequency reconfigurable antennas are widely utilized in modern wireless communication systems due to their ability to dynamically alter frequency characteristics and good electromagnetic compatibility. To satisfy the requirements of miniaturization, broadband, and functional diversification of wireless communication system development, frequency reconfigurable antenna is becoming more and more popular. A large number of frequency reconfigurable antenna have been reported¹⁻⁵, and their reconstruction methods are various. The traditional methods of using PIN diodes and MEMS switches to achieve antenna frequency reconstruction are limited by the inherent size of the switch and the operating frequency band⁶⁻⁹. Because the theoretical design of the variable capacitance of the varactor diode is not quite consistent with the actual, and the experimental design is difficult, the application of the varactor diode in the frequency reconfigurable antenna is relatively limited. The use of LC materials to achieve frequency reconfigurability in the millimeter-wave band is more advantageous than the above methods. Despite the many advantages of LC, many studies based on LCs do not provide measurement results^{10,11}. The above studies do not discuss the design of an antenna structure that can be applied to 5G millimeter wave^{12,13}.

To solve some issues discussed above, in this paper a reconfigurable antenna with parasitic elements, electromagnetic band gap structure and LC is presented. The antenna can achieve wide bandwidth and continuous tunable in 5G millimeter wave band. The paper is organized as follows. Some introductions about the research of reconfigurable antenna are introduced in "Introduction" section. "Operating principle and antenna design" section introduces and analyzes the electromagnetic properties and structure of the reconfigurable antenna. The optimized antenna parameters and corresponding measured outcomes are presented in "Experimental results and discussion" section. Finally, "Conclusion" section provides a conclusion.

Operating principle and antenna design Electromagnetic properties of liquid crystal materials

LC material is a kind of material between liquid and solid, which has both liquid flow characteristics and crystal anisotropy. It can be seen from Fig. 1 that under the control of different external control voltages, the director of the LC molecule determines the dielectric constant tensor in different deflection states^{14,15}.

The relationship between the tensor and the director is as follows¹⁶:

¹School of Ocean Information Engineering, Jimei University, Xiamen 361000, China. ²College of Information and Communication Engineering, Harbin Engineering University, Harbin 150000, China. ✉email: wanglihua@hrbeu.edu.cn

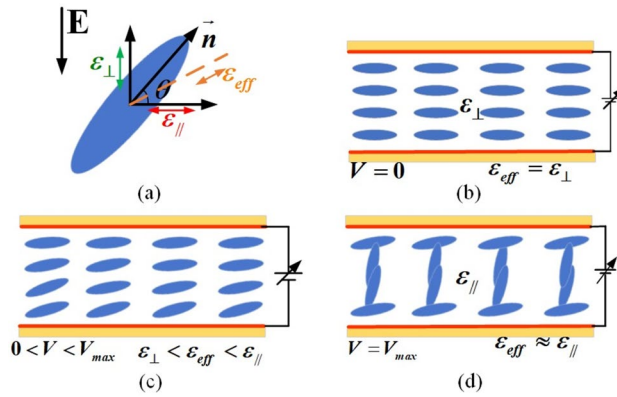


Figure 1. The relationship between the orientation vector of the LC molecule and the applied electric field: (a) the LC molecule's director; (b) alignment of the LC bulk without a bias voltage ($V=0$); (c) with a bias voltage ($0 < V < V_{max}$); and (d) with a saturation voltage ($V \geq V_{max}$).

$$\begin{aligned} \overleftrightarrow{\epsilon} &= \epsilon_{\perp} \cdot \overleftrightarrow{1} + \Delta\epsilon (\vec{n} \otimes \vec{n}) \\ &= \epsilon_{\perp} \begin{bmatrix} 1 & 0 & 0 \\ 0 & 1 & 0 \\ 0 & 0 & 1 \end{bmatrix} + \Delta\epsilon \cdot \begin{bmatrix} n_x^2 & n_x n_y & n_x n_z \\ n_x n_y & n_y^2 & n_y n_z \\ n_x n_z & n_y n_z & n_z^2 \end{bmatrix} \end{aligned} \tag{1}$$

Formula (1), represents the tensor product between the pointing vectors, where $\vec{n} = (\cos\theta, 0, \sin\theta)$, which can be further simplified as:

$$\overleftrightarrow{\epsilon} = \begin{bmatrix} \epsilon_{\perp} + \Delta\epsilon \cos^2\theta & 0 & \Delta\epsilon \sin\theta \cos\theta \\ 0 & \epsilon_{\perp} & 0 \\ \Delta\epsilon \sin\theta \cos\theta & 0 & \epsilon_{\perp} + \Delta\epsilon \sin^2\theta \end{bmatrix} \tag{2}$$

When the applied voltage is 0 V, does not deflect, and the dielectric constant tensor can be expressed as follows:

$$\overleftrightarrow{\epsilon}_{\perp} = \begin{bmatrix} \epsilon_{\perp} & 0 & 0 \\ 0 & \epsilon_{\parallel} & 0 \\ 0 & 0 & \epsilon_{\perp} \end{bmatrix} \quad \overleftrightarrow{\epsilon}_{\parallel} = \begin{bmatrix} \epsilon_{\perp} & 0 & 0 \\ 0 & \epsilon_{\perp} & 0 \\ 0 & 0 & \epsilon_{\parallel} \end{bmatrix} \tag{3}$$

When the applied voltage reaches saturation, the deflection angle becomes 90°. At this point, the LC molecule aligns parallel to the electric field direction, as depicted in Fig. 1c, and its dielectric constant tensor can be simplified to the following formula.

Figure 2 visually demonstrates the change of relative dielectric constant (ϵ_r) and loss tangent ($\tan\delta$) of LC materials with voltage. It can be observed that when the voltage changes within the range of threshold voltage and saturation voltage, the ϵ_r and $\tan\delta$ will also change within the corresponding extreme value.

It can be seen from the figure that the LC molecule will produce elastic deformation in the process of deflection, and the change of energy will deflect the director, thus realizing the frequency switching function. The

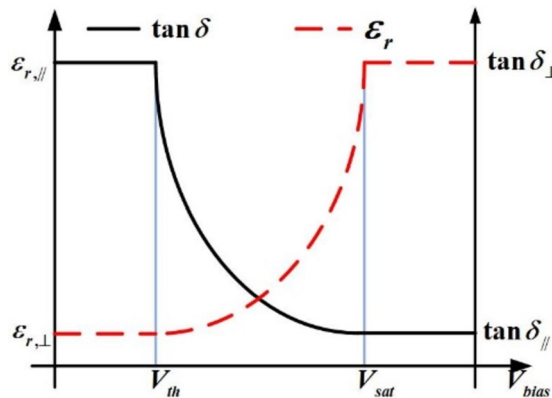


Figure 2. A typical continuous tuning dielectric permittivity and loss tangent \tan versus the bias voltage.

tunability of general tunable materials is usually expressed by ε_r of LC materials. The following formula is the expression of the tuning ability of nematic LC¹⁷:

$$\tau_{LC} = \frac{\varepsilon_{r,\parallel} - \varepsilon_{r,\perp}}{\varepsilon_{r,\parallel}} \quad (4)$$

In the optical field, the anisotropy can be represented by the following formula when LC materials are used in the microwave field because the refractive index can replace the dielectric constant:

$$\Delta n = n_{\parallel} - n_{\perp} = \sqrt{\varepsilon_{r,\parallel}} - \sqrt{\varepsilon_{r,\perp}} \quad (5)$$

According to the Oseen Frank Energy and electromagnetic characteristics related to LC molecules, the famous Freedericksz transition voltage (V_{th}) is a voltage with no molecular reorientation can be reduced derived¹⁸. The threshold voltage can be defined as:

$$V_{th} = \pi \sqrt{\frac{2k_{11}}{\varepsilon_0 \Delta \varepsilon_r}} \quad (6)$$

Antenna design

Figure 3 shows the structure diagram and side view of each layer of the frequency reconfigurable antenna. The overall dimensions of the antenna is $20 \times 25 \times 7.635$ mm³, and the layered structure is adopted. The antenna is mainly composed of three layers, and the specific parameters of each layer are shown in Table 1.

The top layer is the Taconic TLY5 (TM) dielectric substrate with a thickness of 0.381 mm, its dielectric constant is 2.2, and the loss tangent angle is 0.0009. The upper surface of the first layer of the dielectric substrate is etched with a parasitic patch element of 5.5×5.2 mm², and its lower surface is a radiation patch and part of the feeding structure. The four cylindrical through holes with a diameter of 1 mm at the center of the dielectric substrate facilitate the injection of LC using a syringe and the discharge of air during the physical test. The middle layer is a high-frequency dielectric plate with the same ε_r and $\tan \delta$ as the former, and its thickness is 0.254 mm.

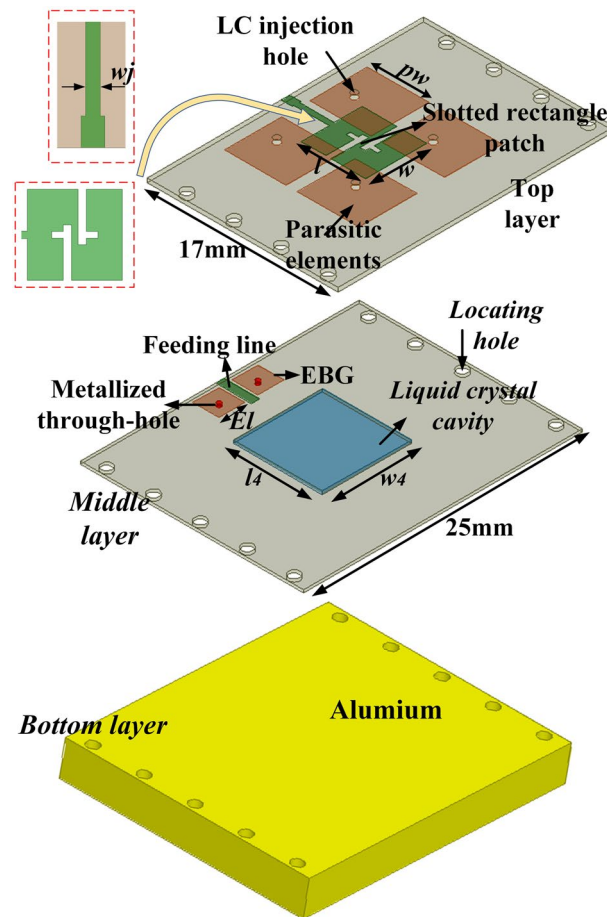


Figure 3. Exploded view and dimension parameters of the proposed antenna. (pw:5.5, w:5.5, l: 5.73, wj:0.46, l4:8, w4:8. Unit: m).

	Front dielectric	LC layer	Back dielectric
Material	Taconic-TLY5(TM)	Rogers5880 LC- BYIPS-P01	Aluminum
Thickness (mm)	0.381	0.254	7
ϵ_r	2.2	2.2 2.74 to 5.4	1
$\tan\delta$	0.0009	0.0009/-	0
Substrate Size(mm ³)	17 × 25 × 0.381	25 × 25 × 0.254	25 × 25 × 7

Table 1. Details of the layers.

The $7 \times 7 \times 0.254$ mm³ cavity in the center of the dielectric substrate of this layer is used for storing LCs, and two electromagnetic band gap structures of the same size and the same distance are placed on both sides of a part of the microstrip structure. The bottom layer is made of a metal aluminum block with a flange through the hole on the side for fixing 2.4 mm RF connector. The cylindrical through-hole with a diameter of 1 mm on both sides of the whole structure is used to fix the multi-layer dielectric substrate. When an external control voltage is applied, an electric field can be formed between the inverted microstrip structure and the aluminum block to control the molecular deflection of the LC.

To further broaden the impedance bandwidth of the antenna, this design uses the principle that parasitic patches can generate new resonance points near the original frequency points and load parasitic patches on the upper part of the upper dielectric substrate. The impact of parasitic patch units on antenna performance is demonstrated in Fig. 4a. Additionally, the return loss has been effectively widened. To further understand the working principle of the parasitic patch, the parameters of the parasitic patch are analyzed. Figure 4b illustrates that a new resonant point can only be generated near the resonant frequency point when the size of the parasitic unit closely matches that of the radiation patch, thereby facilitating spread spectrum effects.

The original microstrip patch antenna and the parasitic patch placed above the main patch form two RLC parallel resonant circuits with the ground, respectively. These two resonant circuits are capacitively coupled through the radiation field of the main patch. Figure 4c demonstrates the equivalent circuit of the additional

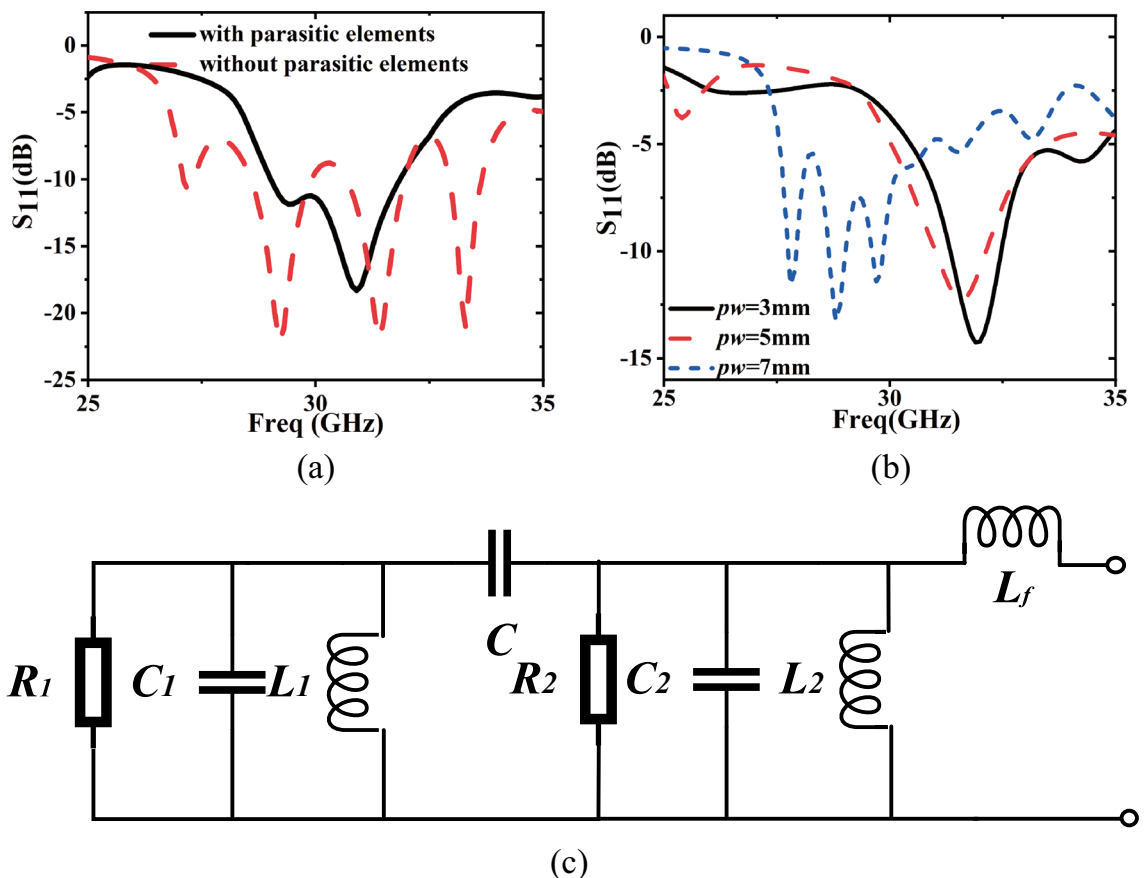


Figure 4. Performance results of parasitic elements. (a) performance comparison. (b) effect of parasitic element length pw . (c) equivalent circuit diagram.

antenna parasitic patch. By modifying the shape, size, and quantity of parasitic elements based on the principle of parasitic elements and equivalent circuits, it is possible to enhance the antenna bandwidth.

Experimental results and discussion

Figure 5 introduces the antenna test scheme and the corresponding physical test process. Deflection of the LC molecules is achieved by applying an external control voltage to both sides of the LC layers through the T-shaped biasing device. The voltage controls achieved the frequency reconfigurable capability.

Figure 6 shows the return loss of simulation and measurement. It can be seen in Fig. 6a with the increase of external control voltage, the resonant frequency point of the antenna decreases from 32.5 to 32 GHz, realizing a shift of 500 MHz. The impedance bandwidth of the antenna remains unchanged throughout the tuning process. Compared with the simulation results in Fig. 6b, the changing trend of return loss is the same, but the offset is different. The measured resonant frequency changes slightly, which is mainly caused by the manufacturing process, measurement error, liquid crystal distribution uniformity and air tightness. In addition, the designed LC antenna did not include a directional layer, which also led to a decrease in antenna tuning capability. The experiment shows that the frequency reconstruction function of the antenna can be realized by adjusting the liquid crystal material with a variable dielectric constant by an electric field.

Antenna resonant frequency versus bias voltage and liquid crystal thickness are shown in Fig. 7. The resonant frequency exhibits variations for varying voltage strengths from 0 to 20 V in Fig. 7a. Consistent with expectations, the resonant frequencies undergo tuning corresponding to the applied voltage. With an increment in the bias voltage strength, the ϵ_{\parallel} increases, whereas the ϵ_{\perp} decreases. Consequently, the resonant frequency shifts towards lower frequencies with an increase in voltage. The threshold voltage value and saturation voltage value are 2 V and 16 V, respectively. Figure 7b illustrates the impact of frequency offset by manipulating the liquid crystal thickness (H) while maintaining ϵ_{\perp} . It is observed that an increase in H results in a decrease in the resonant frequency.

Figure 8 shows the radiation pattern of LC-BYIPS-P01 liquid crystal material on the yz-plane and xy-plane. It can be seen from Fig. 8a that the half power beam width of the antenna is 40° and 42° respectively. And the

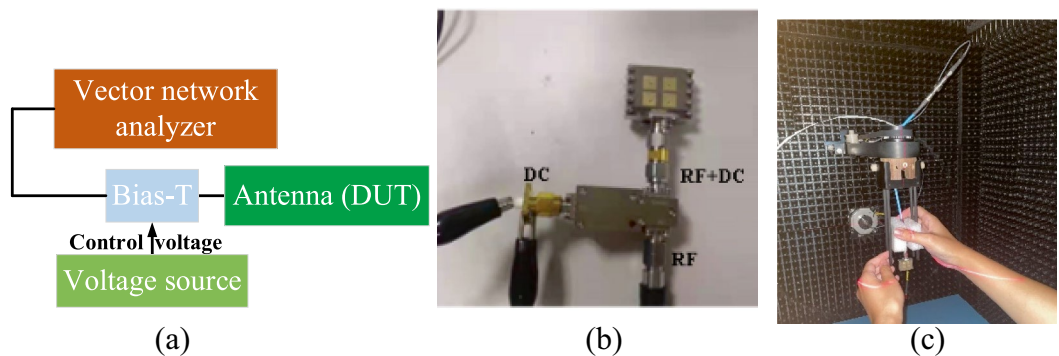


Figure 5. Measurement setup for characteristic evaluation.

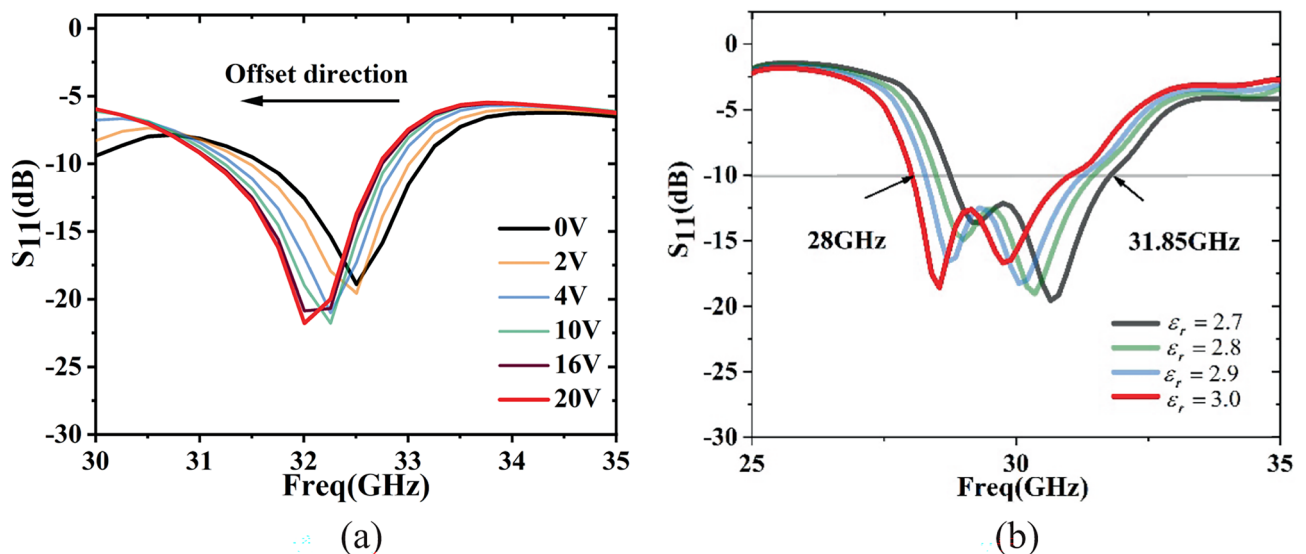


Figure 6. Simulated and measured S-parameters of the fabricated antenna.

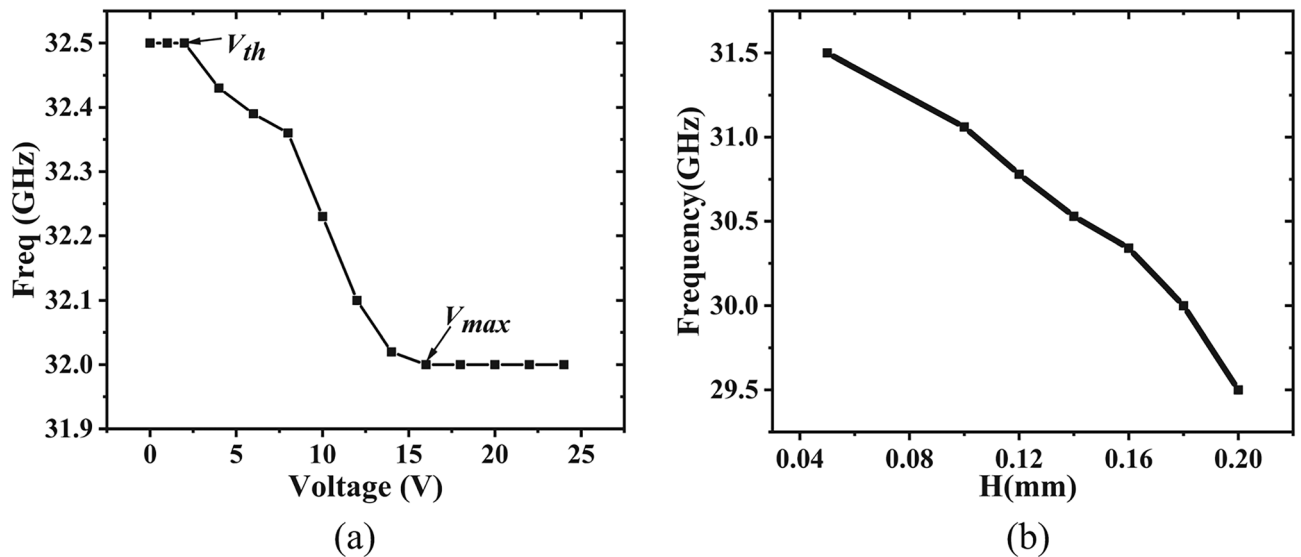


Figure 7. Antenna resonant frequency versus bias voltage and liquid crystal thickness.

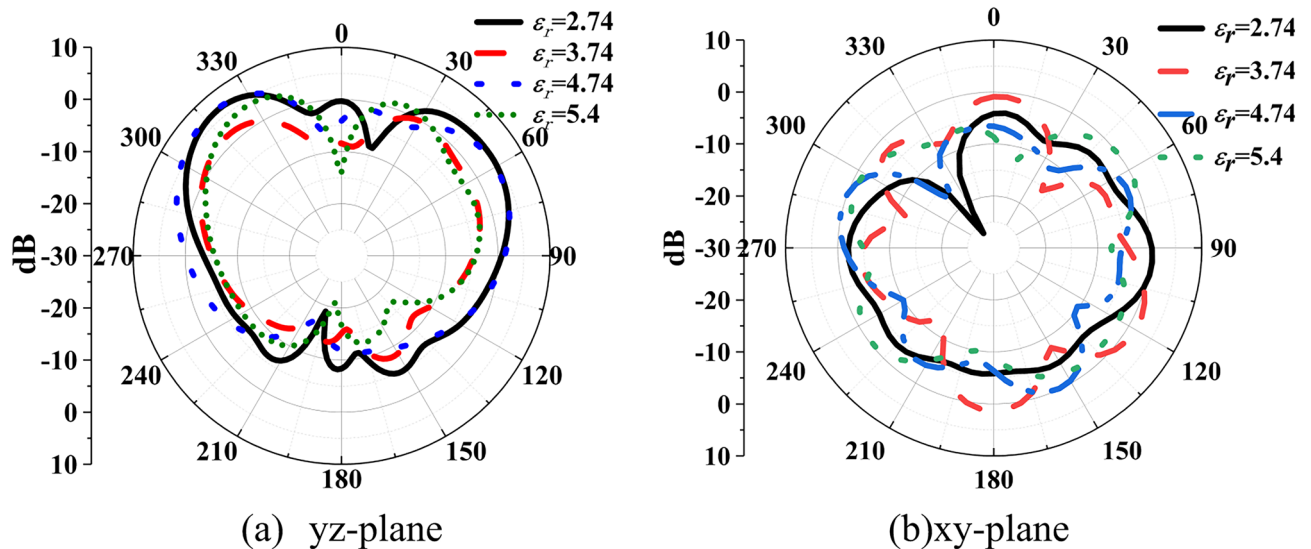


Figure 8. Radiation patterns of yz-plane and xy-plane as a function of anisotropic permittivity of LC.

maximum gain values are 6.25, 5.54 dB. The xy-plane has omnidirectional radiation characteristics. In conclusion, the reconfigurable antenna based on liquid crystal material can not only enable the frequency switching but also keep the radiation characteristics stable during the reconstruction process. Figure 9 shows the simulated peak gain and radiation efficiency. At a dielectric constant of 2.7, the radiation efficiency and gain in the operating band exceed 86.82% and 5.72 dB, respectively. At a dielectric constant of 3, the radiation efficiency and gain in the operating band exceed 92.23% and 4.86 dB, respectively.

Two prior studies used the GT7 LC (Merck KGaA)¹, and K15 LC (Merck)². The electromagnetic properties of these two LCs are, $\epsilon_{r,||} = 3.2$, $\epsilon_{r,\perp} = 2.55$ and $\epsilon_{r,||} = 3.1$, $\epsilon_{r,\perp} = 2.7$. The measurement results obtained from the proposed antenna are compared with the simulations from previous studies^{1,2}, as no existing literature presents the tunable range and reconfigurable bandwidth of LC-based microstrip antennas. Table 2 displays the performance characteristics of the proposed antenna based on LC and the previous antennas. The bandwidths of the antennas are respectively increased by a factor of 2 and 1.5 compared to the LC-based antennas^{1,2}, while the effective sizes of the antennas are 61.4% and 24.6% of those of the previously proposed antennas. It is worth noting that the previously proposed LC-based antenna¹³ does not fully utilize the performance potential of LC, resulting in an inability to operate at 5G millimeter wave.

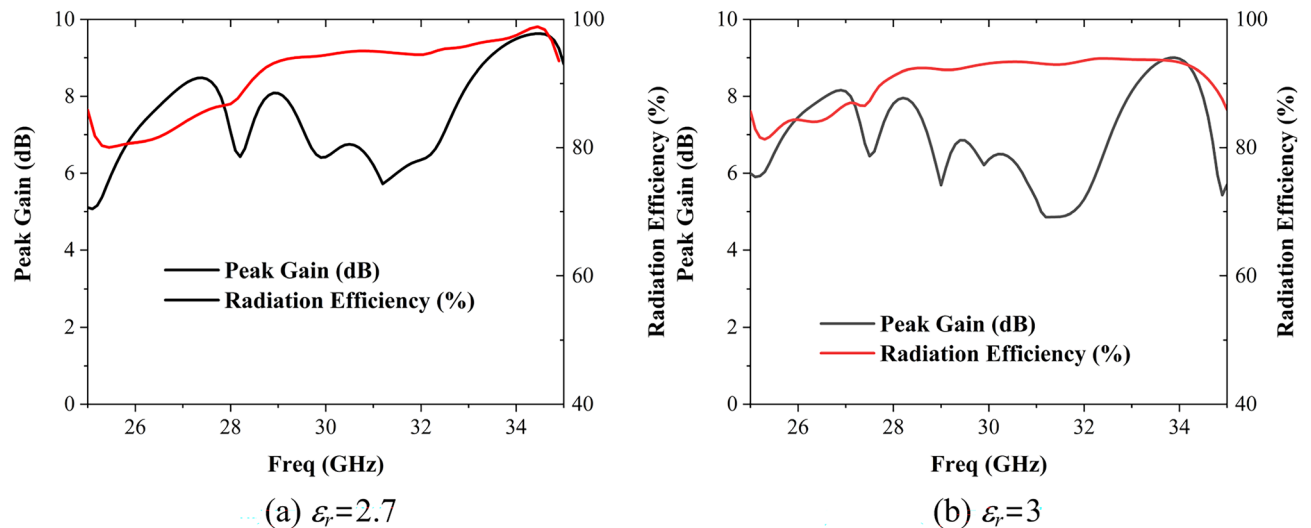


Figure 9. Simulated peak gain and radiation efficiency.

References	Tuning element	Operating band (GHz)	Measured tunable range (GHz)	Effective size (mm ²)
1	LC	29.4–30.4	3	18 × 14
2	LC	27.7–19.5	-	25 × 25
13	LC	2.0–4.0	0.46	50 × 49.7
4	PIN diode	1.79–2.63 3.07–3.61 4.83–5.66	0.2 0.1	115 × 55
Pro	LC	28.8–31.8	0.5	12.9 × 12

Table 2. Compare the design with the antenna of recent years.

Conclusion

A frequency reconfigurable antenna has been designed utilizing LC material. A novel nematic LC, LC-BYIPS-P01, has been introduced into the antenna design. The dielectric constant of the LC is modified by applying a DC voltage, leading to enhanced frequency reconfigurability. Simultaneously, the antenna can be miniaturized using multi-layer technology and slotting technology. Simulation and measurement results demonstrate that the antenna achieves frequency reconfigurability, with a reconfigurable bandwidth of 500 MHz. The proposed antenna is compared with previously developed antennas. The LC utilized in this study exhibits a broader range of adjustable dielectric constants, lower loss tangent, broader bandwidth of the designed antenna, smaller effective size, and improved operation in the 5G millimeter wave band. This design is well-suited for communication systems operating in the 5G millimeter-wave.

Data availability

All data generated or analysed during this study are included in this published article.

Received: 19 January 2024; Accepted: 15 July 2024

Published online: 18 July 2024

References

1. Jaehoon, K. & Jungsuek, O. Liquid-crystal-embedded aperture-coupled microstrip antenna for 5G applications. *IEEE Antennas Wirel. Propag. Lett.* **19**(11), 1958–1962 (2020).
2. Dai, J. W., Peng, H. L., Zhang, Y. P. & Mao, J. F. A novel tunable microstrip patch antenna using liquid crystal. *Progr. Electromagn. Res. C* **71**, 101–109 (2017).
3. Rusan, K. B. & Slawomir, K. Microfluidically frequency-reconfigurable compact self-quadruplexing tunable antenna with high isolation based on substrate integrated waveguide. *Sci. Rep.* **14**, 920 (2024).
4. Chen, P., Wang, L. & Ma, Z. Reconfigurable planar monopole antenna for fifth-generation mobile communication system. *Appl. Comput. Electromagn. Soc. J.* **36**, 67–74 (2021).
5. Li, L., Yan, X., Zhang, H. C. & Wang, Q. Polarization- and frequency-reconfigurable patch antenna using gravity-controlled liquid metal. *IEEE Trans. Circuits Syst. II* (69), 1029–1033 (2022).
6. Boukarkar, A., Lin, X. Q., Jiang, Y. & Yang, X. F. A compact frequency reconfigurable 36-states patch antenna for wireless applications. *IEEE Antennas Wirel. Propag. Lett.* **17**(7), 1349–1353 (2018).
7. Xu, Y. Q., Tian, Y., Zhang, B. Z., Duan, J. P. & Yan, L. A novel RF MEMS switch on frequency reconfigurable antenna application. *Microsyst. Technol.* **24**, 3833–3841 (2018).

8. Jin, X., Liu, S., Yang, Y. & Zhou, Y. A frequency-reconfigurable planar slot antenna using S-PIN diode. *IEEE Antennas Wirel. Propag. Lett.* **21**(5), 1007–1011 (2022).
9. Shynu, S. V. *et al.* Design of compact reconfigurable dual frequency microstrip antennas using varactor diodes. *Prog. Electromagn. Res.* **60**, 197–205 (2006).
10. Zhao, Y., Huang, C., Qing, A. & Luo, X. A frequency and pattern reconfigurable antenna array based on liquid crystal technology. *IEEE Photon. J.* **9**(3), 1–7 (2017).
11. Tae, W. K., Jun, S. P., Seong, O. P. & Senior, M. A. theoretical model for resonant frequency and radiation pattern on rectangular microstrip patch antenna on liquid crystal substrate. *IEEE Trans. Antennas Propag.* **66**(9), 4533–4540 (2018).
12. Ismail, M. Y. & Inam, M. Design of liquid crystal based tunable reflectarray antenna using slot embedded patch element configurations. *Int. J. Electr. Comput. Eng.* **8**(10), 6 (2014).
13. Missaoui, S. & Kaddour, M. Electrically tuned microwave CP cross slot patch antenna using liquid crystal technology”. *Electromagnetics* **39**(3), 158–167 (2019).
14. Wang, Y. L. *et al.* A frequency reconfigurable microstrip antenna based on (Ba, Sr) TiO₃ substrate. *IEEE Trans. Antenna Propag.* **63**, 770–775 (2014).
15. Zhang, W., Li, Y. & Zhang, Z. A reconfigurable reflectarray antenna with an 8 μ m-thick layer of liquid crystal. *IEEE Trans. Antennas Propag.* **70**, 2770–2778 (2022).
16. Apala, M. & Arghir, Z. Landau-de Gennes theory of nematic liquid crystals: The oseen-frank limit and beyond. *Arch. Ration. Mech. Anal.* **196**, 227–280 (2010).
17. Maune, H., Jost, M., Reese, R. & Polat, E. Microwave liquid crystal technology. *Crystal* **8**, 355 (2018).
18. Takikawa, Y. *et al.* Freedericksz transition in a dual-frequency nematic liquid crystal. *Jpn. J. Appl. Phys.* **59**, 041006 (2020).

Acknowledgements

This work was supported by the Natural Science Key Foundation of Fujian Province Grant with No.2020J02042, and the Natural Science Foundation of Fujian Province of China Grant with No. 2021J05179, and the National Foundation Cultivation Program Project of Jimei University Grant with No. ZP2021011.

Author contributions

Conception, design, data collection, analysis, simulation, and measurement were initially carried out by Peng Chen, Dan Wang, and Lihua Wang. All authors contributed to complete the writing and presentation of the whole manuscript.

Competing interests

The authors declare no competing interests.

Additional information

Correspondence and requests for materials should be addressed to L.W.

Reprints and permissions information is available at www.nature.com/reprints.

Publisher's note Springer Nature remains neutral with regard to jurisdictional claims in published maps and institutional affiliations.



Open Access This article is licensed under a Creative Commons Attribution-NonCommercial-NoDerivatives 4.0 International License, which permits any non-commercial use, sharing, distribution and reproduction in any medium or format, as long as you give appropriate credit to the original author(s) and the source, provide a link to the Creative Commons licence, and indicate if you modified the licensed material. You do not have permission under this licence to share adapted material derived from this article or parts of it. The images or other third party material in this article are included in the article's Creative Commons licence, unless indicated otherwise in a credit line to the material. If material is not included in the article's Creative Commons licence and your intended use is not permitted by statutory regulation or exceeds the permitted use, you will need to obtain permission directly from the copyright holder. To view a copy of this licence, visit <http://creativecommons.org/licenses/by-nc-nd/4.0/>.

© The Author(s) 2024